



Heterocyclic-based Schiff base material designed as optochemical sensor for the sensitive detection of chlorinated solvent vapours

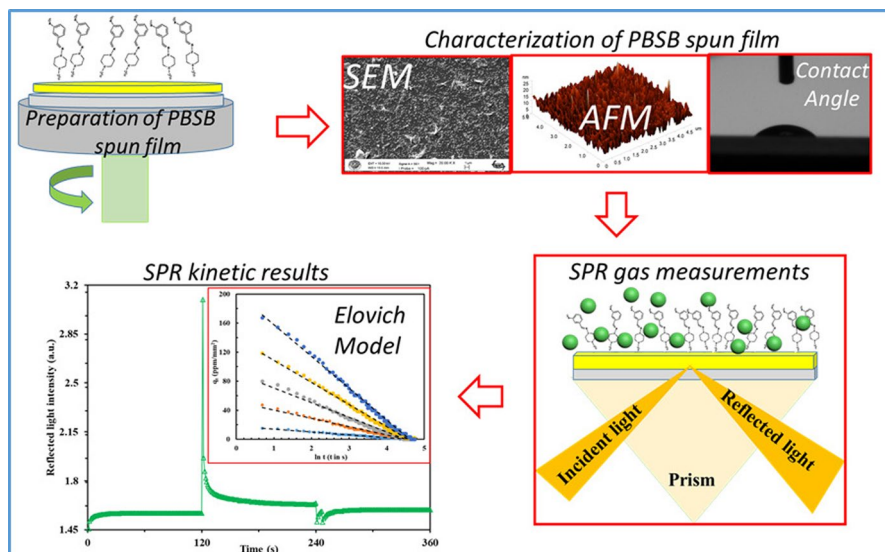
Erkan Halay^{1,2} · Inci Capan³ · Rifat Capan³ · Emriye Ay⁴ · Yaser Acikbas⁵

Received: 15 May 2024 / Accepted: 20 July 2024 / Published online: 27 July 2024
© The Author(s) 2024

Abstract

Herein, a newly synthesized intermediate, piperazine-based Schiff base (PBSB) gas sensor was fabricated by the Schiff base condensation of amino functionalized methylpiperazine with aromatic aldehyde containing nitro substituent. This organic sensor material was structurally identified with spectroscopic techniques such as FTIR, HRMS, ¹H- and ¹³C-NMR. The designed sensor candidate was explored for its optical response to chlorinated volatile organic compounds, namely trichloroethylene, dichloromethane and chloroform in the light of structure–property relationship investigation by using surface plasmon resonance (SPR) technique. The results showed that Schiff bases could be candidates for chlorinated vapour sensing materials with their good response and reversibility. Concordantly, compound PBSB exhibited good response against chlorinated solvent vapours aided by the electron-withdrawing group on benzene ring that promoted better intermolecular interactions and opened up a new strategy to create a novel set of responsive materials for gas sensing applications. In addition, the adsorption kinetics of SPR data obtained from PBSB spun film on exposure to these chlorinated vapours at different concentrations was also evaluated using the Elovich Model. The values of the initial adsorption rate, *a* and Elovich constant, *b* were analysed depending on the concentration values and the highest values were obtained for dichloromethane between 372.92 and 4377.53 ppm/mm².

Graphical abstract



Keywords Schiff base · Piperazines · Optochemical sensor · Chlorinated vapours · Elovich model

Introduction

Because of serious environment contamination of chemical agents and their highly adverse and potentially fatal effects on human health, various technologies have still been developed to detect those species and/or transform them into un-hazardous substances [1–3]. Among those agents, volatile organic compounds (VOCs) which are in the spotlight, have come to the forefront with many different fields such as quality analysis of food and beverage, disease detection, life science and particularly security/environmental/atmospheric research along with industrial processes [4–6]. In this sense, although the health risk level varies greatly, many VOCs may have an adverse footprint on the environment and pose a notable health risk (mutagenic, genotoxic, teratogenic, carcinogenic) to human being as a result of long term exposure [7]. Of these, chlorinated volatile organic compounds (CVOCs) arise from a number of outdoor and indoor sources such as emissions of various industrial processes as well as household products such as office supplies, cleaning products woods and insulating materials. And as the fact is already known that people spend approximately 90% of their time indoors and that indoor air is often more polluted than outdoor air due to inadequate ventilation, it is clear that such CVOCs are hazardous to the human health. Therefore, detection, analysis and characterization of those VOCs have played a crucial role for a better quality of human life [8–10].

Mass coupled large-scaled laboratory instruments such as high-performance liquid (HPLC) and gas chromatography (GC) have been widely used for the conventional characterization of a wide variety of VOCs as those compounds exist in such low concentrations that is made to be hardly detected [11, 12]. However, these powerful and versatile techniques have some limitations/challenges such as requiring sample collection, long analysis duration, high cost, expensive instrumentation/equipment, trained operator and fixed testing environment (off-line testing) and hence limited their general use and real time on-site monitoring [13, 14].

For those reasons, as an alternative approach in the current quarter century, the mass sensitive devices have had an ongoing popularity among many kinds of sensors which have been developed for gas detecting. Amongst them, quartz crystal microbalance (QCM) and surface plasmon resonance (SPR) techniques, which used thin films of organic/inorganic materials prepared by physical/chemical methods such as spin coating, vapour deposition and Langmuir–Blodgett deposition techniques, have been being in the centre of attention due to the advantages including excellent sensitivity, selectivity, stability and fast response, as well as facile use [15–18]. Those which, SPR sensors have been favoured due to many advantages such as convenient production, high sensitivity and wide application with dozens of organic and inorganic materials fabricated as sensor candidates until today [19, 20]. However, SPR sensor-based research efforts have mainly focussed on the detection of common VOCs such as toluene, benzene, xylene and formaldehyde [21–23]. Therefore, relevant works on chlorinated solvent vapour sensing are quite rare and it has been imperative to develop new SPR coating sensor chip that is rich with the interaction sites.

In this context, as one of the most popular organic intermediate compounds formed by nucleophilic addition reaction between aldehydes and primary amines, Schiff bases have a wide range of applications such as biological molecules, various types of sensors, coordination compounds and catalysts [24–27]. The features that enable them to have this quality are the imine ($-C=N-$) group that breaks the molecular symmetry, and the conjugation, if any. Especially, Lewis base qualified related nitrogen atoms interact with target species as a recognition site via acid/base, hydrogen bonding and such intermolecular interactions to enhance the sensor ability [28, 29].

In the light of the foregoing aspects and in continuation of our efforts to discover chemical sensors in different fields/disciplines [30–33], an imine model was thought and designed based on piperazine heterocycle. Hereby, as the main motivation for our future works and prospects along with the inconvenience of being limited number of reports available in the literature on gas sensors with Schiff bases, we introduce a new Schiff base, 4-methyl-N-(3-nitrobenzylidene)piperazin-1-amine synthesized and explored as a sensitive gas sensor that may open up a new strategy for exploring a set of novel, responsive materials towards gas sensing applications.

Experimental details

Materials and measurements

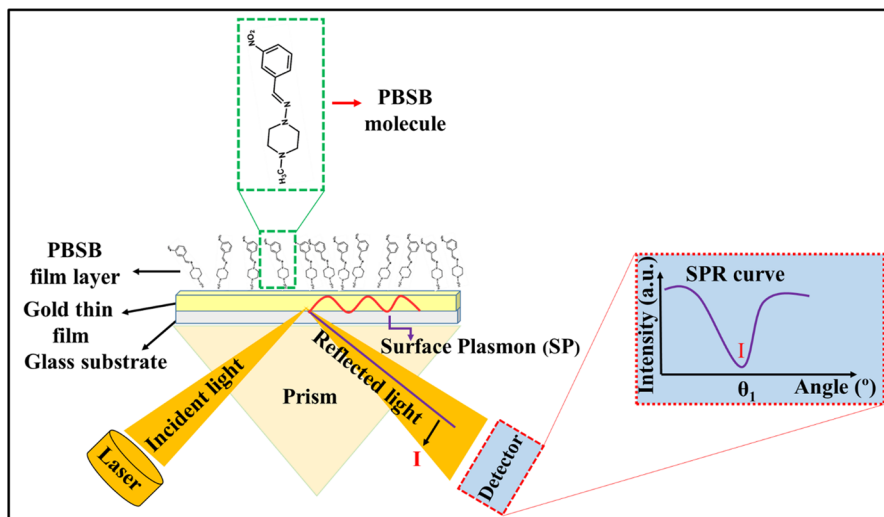
All starting reagents for the synthesis of PBSB, and solvents mentioned in the synthesis, characterization studies and sensing applications were purchased from Sigma-Aldrich, Merck, Alfa Aesar and Acros Organics and were employed without further treatment. Oven-dried double neck flask was used under nitrogen atmosphere to perform the reaction. The related reaction was also monitored by thin-layer chromatography (TLC) application using classical aluminium supported sheets coated with silica gel 60 along with fluorescent indicator F₂₅₄ (Kieselgel 60 F₂₅₄) and 254 nm UV lamp was used to visualize the spots of the compounds. Melting point (uncorrected data) of PBSB was obtained using Gallenkamp Electrothermal apparatus. Infrared spectrum of sample in thin-film form was measured on a PerkinElmer Spectrum Two FTIR spectrophotometer equipped with an ATR accessory. NMR experiments including ¹H- and ¹³C-NMR were performed on a Varian Mercuryplus AS 400 spectrometer and reported in units of parts per million (ppm) relative to tetramethyl silane ($\delta=0$ ppm) as internal standard and the residual solvent signal CDCl₃ ($\delta=7.26$ ppm for ¹H- and $\delta=77.0$ ppm for ¹³C-NMR). High-resolution mass spectrometry (HRMS) data were obtained on an Agilent 6530 Q-TOF LC/MS instrument featuring jet stream electrospray ionization source in positive ion mode.

Synthesis of piperazine-based Schiff base sensor compound

3-nitrobenzaldehyde (3-NBA; 5.66 mmol) and 25 mL of anhydrous ethanol (EtOH) were introduced into the flask from which the air was removed by purging with N₂ before. Afterwards, 1-amino-4-methylpiperazine (AMPRZ; 0.75 mL, 6.23 mmol) was slowly added to this solution with continuous stirring and the reaction mixture was refluxed for 5 h. Following the reaction completion by TLC check and cooling, the resultant precipitate was collected by filtration and then washed with cold ethanol to remove impurities. Thus, piperazine-based Schiff base (PBSB) was synthesized (yellow solid, 1.26 g, 90% yield) as depicted in Scheme 2. M.p: 104–106 °C, FTIR (ATR, cm⁻¹) ν 3079 (=C–H), 2983, 2948, 2931, 2846, 2796 (cycloalkane/aliph. CH), 1585 (C=N), 1519, 1350 (N–O), 1456, 1440 (arom. C=C), 1160 (C–N). ¹H NMR (400 MHz, CDCl₃) δ _H 8.37 (t, 1H, N=CH), 8.02 (dq, 1H, ArH), 7.84 (dt, 1H, ArH), 7.46 (s, 1H, ArH), 7.44 (t, 1H, ArH), 3.23 (t, 4H), 2.58 (t, 4H), 2.33 (s, 3H). ¹³C-NMR (100 MHz, CDCl₃) δ _C 148.6, 138.3, 131.6, 131.3, 129.2, 122.0, 120.5, 54.3, 50.6, 45.9. HRMS (ESI-TOF) calcd for C₁₂H₁₇N₄O₂ [M+H]⁺ 249.1351, found 249.1347.

Surface plasmon resonance (SPR) technique

The SPR system is based on the principle of energy transfer between metal electrons on a well-conducting metal-coated surface (gold, silver, copper, etc.) and electromagnetic waves sent to the surface. When energy transfer occurs between the metal



Scheme 1 Schematic illustration of SPR technique used for the gas measurements

surface and the transmitted electromagnetic waves, a change in the intensity of the light reflected from the underside of the metal surface occurs. Surface plasmon resonance is determined when the change in the light intensity is measured. When light is sent at different angles to the metal surface, some of the light is reflected and some is absorbed. This angle, which depends on the reflected light intensity, is called the resonance angle.

To generate surface plasmons during SPR measurements, a prism-based SPR system known as the Kretschmann configuration system was used. In this study, all gas sensing measurements were performed using the Biosuplar 6 Model SPR setup with the Kretschmann configuration. All configurations were designed to directly, simultaneously, and without any labelling process measure the change in refractive index at the sensor surface. A schematic representation of the SPR system used in this work is given in Scheme 1. A polarized beam of light from a HeNe laser with a wavelength of approximately 633 nm is sent to the prism. On the prism, the polarized beam advances through the gold thin film of approximately 50 nm thickness formed on the glass surface and the thin film to be examined on the gold film surface. A liquid of the same index as the glass is applied between the glass and prism to ensure optical coupling. When the polarized beam encounters the gold film and the thin-film interface on the surface of the gold film, total internal reflection occurs. In this case, as long as the angle of incidence is greater than the critical angle, waves of decreasing amplitude continue to be generated. Usually, the intensity of the reflected light does not change with the angle of incidence under the condition of total internal reflection. At an angle greater than the critical angle, the incident wave excites the delocalized electrons of the gold film, bringing them into resonance. In this state, maximum energy is absorbed and surface plasmon resonance occurs. The intensity of the reflected light decreases sharply at this point, and the angle of incidence at which minimum reflection is observed is called the resonance angle or SPR (θ) angle.

Elovich model

The basic theory of the Elovich model is described as follows: (i) The activation energy is increased with the adsorption time and (ii) the surface of the adsorbent is heterogeneous [34]. This model is widely used to study the adsorption behaviour of solid thin films during the interaction between a solid surface and adsorbents. For the SPR kinetic measurement during the adsorption dynamics between thin-film sensor and vapour molecule, the adsorption capacity (the adsorption amount per unit area), q_t , is described for the first time as [35]:

$$q_t = \left[\frac{(I_i - I_e)V}{A} \right] \quad (1)$$

where I_i is the initial reflected light intensity, I_e is the equilibrium reflected light intensity, V is the injected vapour volume and A is the thin-film surface area, respectively.

The adsorption rate (dq_t/dt) for the Elovich model is described as [36]:

$$\frac{dq_t}{dt} = a \exp(-bq_t) \quad (2)$$

where a is the initial adsorption rate, b is the Elovich desorption constant and q_t is the quantity of gas adsorbed at time t , respectively. When q_t is chosen 0, Eq. 2 is equal to a which is regarded as the initial adsorption rate. If the boundary conditions can be chosen from $q_t = 0$ at $t = 0$ and $q_t = q_t$ at $t = t$, Eq. 2 can be integrated as [37]:

$$q_t = \left(\frac{1}{b} \right) \ln(ab) + \left(\frac{1}{b} \right) \ln t \quad (3)$$

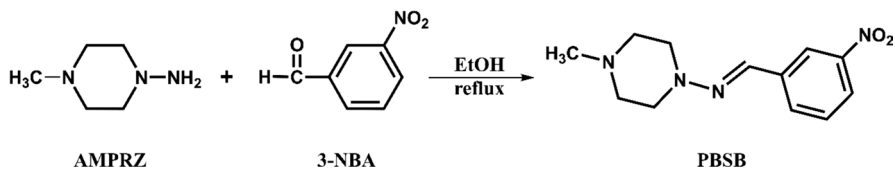
Equation 3 can be adapted to experimental results, and it is suitable to determine such constants a and b which are used to explain the nature of vapour adsorption onto a thin-film surface.

If we assume $t \gg t_0$, the validity of Eq. 3 can be checked by plotting q_t versus $\ln t$ that gives a linear relationship. By using the intercept $(\frac{1}{b}) \ln ab$ and the slope $(\frac{1}{b})$ of this relationship the a and b values can be calculated [38]. The correlation coefficient (R^2) of this graph gives us an indicator of the conformity between SPR experimental adsorption data and the Elovich model prediction.

Results and discussion

Design, synthesis and chemical characterization of PBSB

The imine nitrogen atoms acting as Lewis bases in Schiff base compounds interact with the target species via hydrogen bonding and/or various electrostatic intermolecular interactions to enhance the sensing ability of sensor molecule. Those kinds of compounds have also drawn considerable interest in the field of



Scheme 2 Synthetic pathway of piperazine-based Schiff base PBSB synthesis

pharmaceutical sciences and coordination chemistry as well as gas sensors that operate on the basis of the electronic configuration modification/optical properties in the presence of its analyte gas. In this context, as the main motivation for our work, it was thought that Schiff base functionalized organic compounds provided by the combination of structural features of piperazine heterocycle along with the electron-withdrawing substituted aromatics would exhibit synergistic benefits about gas sensing.

Accordingly, as stated in our previous work in the literature [39], by the condensation of amino functionalized, methylated piperazine derivative (AMPRZ) with nitro group substituted benzaldehyde skeleton (3-NBA) afforded the sensor candidate PBSB as shown in Scheme 2. The chemical structure establishment was confirmed with Fourier-transform infrared (FTIR), proton and carbon nuclear magnetic resonance (^1H -, ^{13}C -NMR) spectroscopic techniques along with high-resolution mass spectrometry (HRMS).]

The FTIR spectrum of PBSB showed a moderately intense absorption peak assigned to a stretching band of the iminic $\text{C}=\text{N}$ at 1585 cm^{-1} and a weak absorption peak of the iminic hydrogen ($\text{H}-\text{C}=\text{N}$) at 3079 cm^{-1} , along with aldehyde and amino groups stretching bands disappearance for the evidence of starting materials consumption (Fig. S1) [40]. These characteristic peaks matched well with NMR spectrums, as ^1H and ^{13}C -NMR experiments showed the signal for iminic proton at 8.31 ppm, while the signal for azomethine carbon at 166.3 ppm, confirming the formation of imine condensation (Figs. S2-S3) [41]. In addition to those, HRMS spectrum of the model compound PBSB exhibited $[\text{M} + \text{H}]^+$ ion peak as 249.1347 m/z corroborating the proposed structure of PBSB in accordance with the calculated molecular ion value (Fig. S4).

Characterization of the PBSB thin films

AFM and SEM images were obtained to reveal the nanometric structure of PBSB thin films. Figure 1a and b shows 2D and 3D images of PBSB thin films coated on the glass surface. By analysing the image in Fig. 1a and b, it was obtained on a $5 \times 5\text{ }\mu\text{m}$ scale that the area roughness and root-mean-square (rms) are 1.85 nm and 2.28 nm for PBSB film, respectively. This film is homogeneous and smooth despite the high peaks in some areas. In addition, SEM images in Fig. 1c and d showed that the morphologies of the bare glass substrate and the PBSB-coated

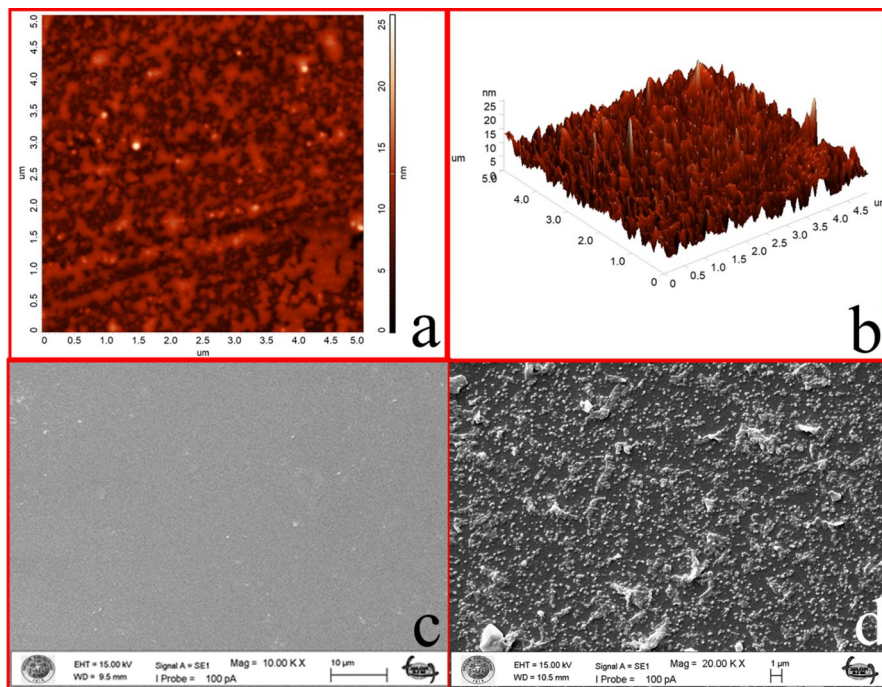


Fig. 1 **a** 2D and **b** 3D AFM images of PBSB-coated substrate **c** SEM image of bare glass substrate **d** SEM image of PBSB-coated substrate

glass surface were different and PBSB molecules were homogeneously distributed on the surface. The wettability of the surfaces was also examined by contact angle measurements, and the water contact angles of the bare glass and PBSB-coated surfaces were found to be $22.32^\circ \pm 1.23$ and $47.61^\circ \pm 0.95$, respectively (Fig. 2). The fact that there are amine/imine functional groups that increase hydrophilicity in the structure of the PBSB molecule confirms these results.

Gas Sensing properties of the PBSB thin films

All kinetic measurements of the spun thin film formed from PBSB material were made at room temperature by using a syringe. Initially, the PBSB thin-film sensor was exposed to dry air for 120 s. At the 120th second, organic vapour was pumped at saturated concentration and the organic vapour PBSB thin-film sensor was allowed to interact for 120 s. Followingly, dry air was pumped into the gas cell again at the 240th second to remove the organic vapour from the environment. This process was repeated separately for 3 individual organic vapours (dichloromethane, chloroform and trichloroethylene), and the kinetic measurements of the PBSB thin-film sensor are given in Fig. 3. In this figure, it is

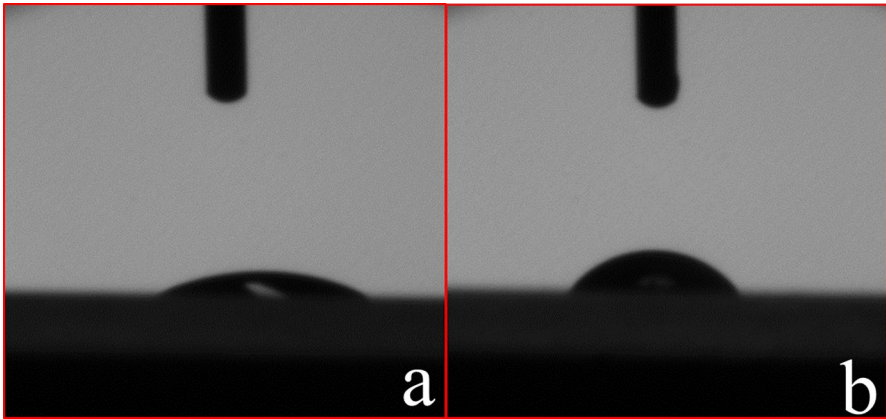


Fig. 2 Contact angle measurements of **a** bare glass substrate and **b** PBSB-coated glass substrate

schematically indicated that the harmful organic vapour molecules attempt to diffuse into the PBSB thin film during the time interval of 120–240 s.

The ideal kinetic response should have the sensor characteristics with low response and recovery times, high sensitivity, low limit of detection (LOD) and limit of quantification (LOQ). These sensor parameters are listed in Table 1 for the PBSB thin-film sensor. Response time for all vapours was only 2 s and recovery times were found to be between 5 and 8 s, of which is very low. The response for the increasing amount of the vapour per ppm of the vapour molecules, namely sensitivity, was obtained by using the kinetic graphs. The sensitivity, LOD and LOQ values were calculated as in the methodology reported in our previous study [42] and are presented in Table 1. LOD and LOQ values were found to be in the order of a few ppm. The regression coefficient (R^2) for the calibration of the data was close to unity. To

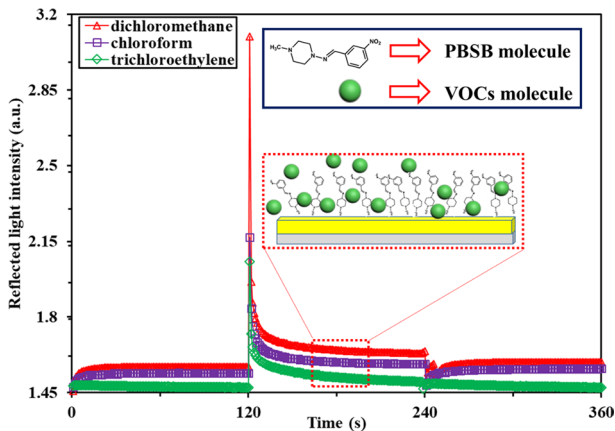


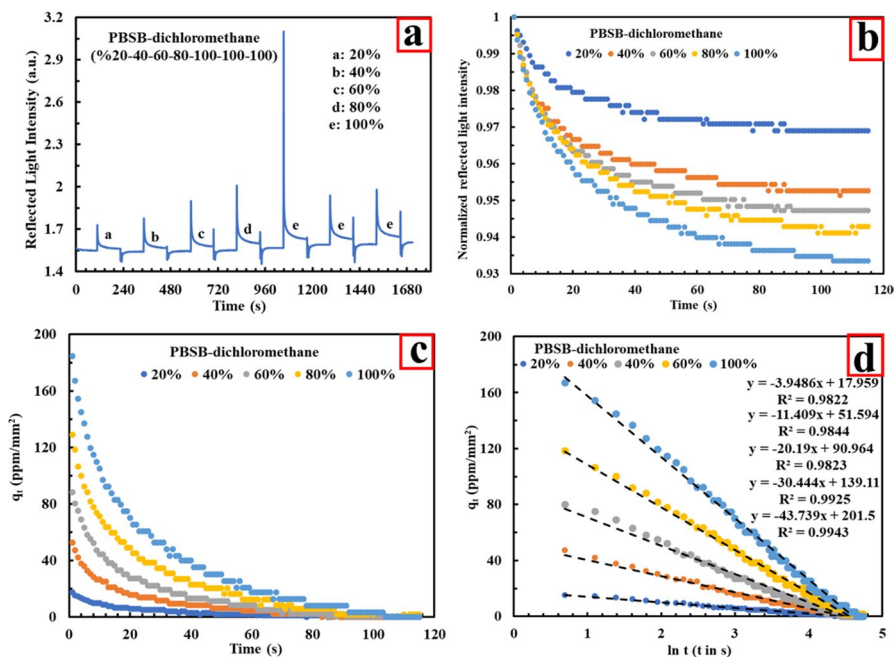
Fig. 3 Kinetic response of PBSB thin-film sensors against different VOCs

Table 1 Sensor parameters for the PBSB thin-film sensor

CVOCs	Response time (s)	Recovery time (s)	Sensitivity (Response/ppm) $\times 10^{-3}$	LOD (ppm)	LOQ (ppm)	R ²
Dichloromethane	2	5	1.78	1.85	5.62	0.9749
Chloroform	2	8	2.27	1.45	1.94	0.9617
Trichloroethylene	2	5	1.70	1.94	5.88	0.9651

calculate these values, calibration curves of PBSB SPR sensors as a result of the exposure to increasing concentrations of the chlorinated vapours were plotted using the kinetic data and are given in Fig. S5.

PBSB thin film is also exposed to dichloromethane, chloroform and trichloroethylene vapours using different concentration ratios (20%, 40%, 60%, 80% and 100%). The thin-film response to all vapours is given in Fig. 4, Figs. S6-S7 (a). Adsorption dynamics are investigated when the vapour is injected into the gas cell until removing the vapour from the gas cell. Figure 4 and Figs. S6-S7b indicate normalized reflected light intensity as a function of time. The vapour response rate of all samples increased when the amount of each concentration increased. Equation 1 is used to calculate q_t value given in Fig. 4, Figs. S6-S7c and q_t values versus time yields a fast decrease because of an interaction between the PBSB thin film and vapour

**Fig. 4** Adsorption results of PBSB thin film for dichloromethane vapour

molecules. Equation 3 and Fig. 4, Figs. S6-S7d are used for Elovich model to determine a and b constants which are given in Table 2. The Elovich model gave a linear relationship with high correlation coefficients. It can be concluded that the adsorption kinetic data yields a best fit to the Elovich model due to a linearly increasing energy of adsorption with the surface coverage [34, 43].

A comparison of results for each concentration of three organic vapour is also given in Table 2. It can be noticed that a values increased and b values decreased when each concentration value increased. The highest value of a is found for dichloromethane and the lowest value of a is observed for trichloroethylene vapour. The exact opposite situation is observed for b values. It is well known that adsorption process begins when vapour molecules reach the film surface and then enter into the thin-film structure.

The molar mass and vapour pressure properties of VOCs play an important role for the adsorption process between the sensing material and vapour molecules. The molar mass values of organic vapours are 84.93 g/mol (dichloromethane), 119.38 g/mol (chloroform) and 131.38 g/mol (trichloroethylene). The vapour pressure values are 57.3 kPa at 25 °C, 25.9 kPa at 25 °C and 7.8 kPa at 20 °C for dichloromethane, chloroform and trichloroethylene, respectively.

Dichloromethane vapour has the lowest molar mass amongst chloroform and trichloroethylene vapours. Concordantly, dichloromethane vapour molecule is the leading candidate to enter into the thin-film structure among two other vapour molecules [44]. If we compare the vapour pressure values, dichloromethane has the highest value among others. That means dichloromethane vapour generated higher vapour pressure onto the film surface, when compared with the other vapours [45].

Table 2 Adsorption results of PBSB thin film for three different organic vapours

Organic vapour	C (%)	Fitting Equation	R^2	Elovich Constant	
				a (ppm/mm ²)	b (mm ² /ppm)
Dichloromethane	20	$y = -3.9486x + 17.959$	0.9822	372.9176	0.2532
	40	$y = -11.409x + 51.594$	0.9844	1049.845	0.0876
	60	$y = -20.19x + 90.964$	0.9823	1826.549	0.0495
	80	$y = -30.444x + 139.11$	0.9925	2936.232	0.0328
	100	$y = -43.739x + 201.5$	0.9943	4377.530	0.0228
Chloroform	20	$y = -2.8168x + 13.27$	0.9864	313.1239	0.3550
	40	$y = -6.437x + 29.013$	0.9744	583.5076	0.1553
	60	$y = -14.226x + 64.965$	0.9885	1367.944	0.0702
	80	$y = -19.833x + 91.606$	0.9924	2008.904	0.0504
	100	$y = -30.139x + 138.18$	0.9921	2950.759	0.0331
Trichloroethylene	20	$y = -1.956x + 9.4279$	0.9755	242.231	0.5112
	40	$y = -3.427x + 14.717$	0.9181	251.055	0.2918
	60	$y = -11.339x + 50.61$	0.9744	980.676	0.0881
	80	$y = -12.809x + 59.438$	0.9828	1326.244	0.0780
	100	$y = -29.995x + 138.78$	0.9962	3062.490	0.0333

a value gives the amount of adsorbed vapour in ppm for per surface area in mm^2 . In this respect, the values of adsorbed chlorinated vapour for per surface area given in Table 2 can be compared in terms of some physical properties such as molar volumes and vapour pressures. Considering the a values calculated for five different concentration values of organic vapours, it is seen that DCM vapour has higher values of adsorbed vapour amount per surface area compared to other vapours. This may be attributed to the fact that DCM vapour has relatively the highest vapour pressure and the lowest molar volume. Thus, DCM vapour molecules can relatively penetrate into the PSBS film more easily. This easy penetration leads to an increase in the amount of adsorbed organic vapour per surface area.

Conclusions

A large number of adsorbent organic materials have been being synthesized by many researchers and the environmental effect on their adsorption features like temperature, concentration and substituent groups of main frameworks have been being continued to be investigated. To the best of our knowledge, as an organic compound, Schiff bases have been used less than other organic materials in this context, and as virgin compounds, they deserve much more attention in the literature with their high gas sensor potential. Within this scope, in conclusion, a Schiff base compound was prepared as a sensor candidate in order to detect chlorinated solvent vapours such as chloroform, dichloromethane and trichloroethylene. In order to illuminate some characteristic properties of PSBS SPR sensor the values of sensitivity, LOD, LOQ and response-recovery times were also calculated. The values of the sensitivity, LOD and LOQ for the chlorinated solvent vapours found to be between 1.70 and 2.27. $\text{response/ppm} \times 10^{-3}$, 1.45–1.94 and 1.94–5.88 ppm, respectively. Besides, the response and recovery times for chlorinated solvent vapours were found to be between 2 s and 5–8 s, respectively. PBSB exhibited superior chlorinated solvent sensing ability at room temperature, including high response and excellent reversibility. It is concluded that the imine nitrogen-halogen interaction between PBSB molecule and chlorinated VOCs plays a key role in the superior sensing property. In addition, Elovich model was used to study the adsorption behaviour of PBSB SPR sensor during the interaction between PBSB molecule and applied vapour molecules. In this regard, the conformity between SPR experimental adsorption data and the Elovich model prediction was obtained. The validity of this model was confirmed by using the correlation coefficient (R^2) value as an indicator of the conformity between the model prediction and experimental adsorption data. The values of the correlation coefficient were obtained for the saturated concentration of dichloromethane, chloroform, and trichloroethylene vapour as $R^2 = 0.9943$, $R^2 = 0.9921$, and $R^2 = 0.9962$, respectively. In addition, the values of the initial adsorption rate, (a) were calculated range from between 372.92–4377.53, 313.12–2950.76, and 242.23–3062.49 ppm/mm^2 for dichloromethane, chloroform, and trichloroethylene vapours, respectively. In addition, the Elovich constant, that were obtained as b values range from 0.2532–0.0228, 0.3550–0.0331, to 0.5112–0.0333 $\text{mm}^2/\text{s/ppm}$ for dichloromethane, chloroform, and trichloroethylene vapours, respectively. These

values obtained for b constant showed an inversely proportional relationship with the amount of concentration applied to the PBSB film sensor. This work gives a reasonable interpretation on the adsorption properties of Schiff bases and introduces the imine structure as an important factor for the fabrication and detection of molecules with different substituents.

Supplementary Information The online version contains supplementary material available at <https://doi.org/10.1007/s11164-024-05359-6>.

Acknowledgements Atatürk University, Eastern Anatolia High Technology Application and Research Centre (DAYTAM) is gratefully acknowledged for spectrometric analysis.

Author contributions EH contributed to the investigation, formal analysis and writing—original draft. IC was involved in conceptualization, methodology, review and editing. RC contributed to the investigation, formal analysis, data curation and investigation. EA contributed to investigation, validation and formal analysis. YA was involved in supervision, writing—review and editing.

Funding Open access funding provided by the Scientific and Technological Research Council of Türkiye (TÜBİTAK).

Data Availability No datasets were generated or analysed during the current study.

Data and code availability Data will be made available on reasonable request.

Declarations

Conflict of interest The authors declare no competing interests.

Ethical approval Not applicable.

Open Access This article is licensed under a Creative Commons Attribution 4.0 International License, which permits use, sharing, adaptation, distribution and reproduction in any medium or format, as long as you give appropriate credit to the original author(s) and the source, provide a link to the Creative Commons licence, and indicate if changes were made. The images or other third party material in this article are included in the article's Creative Commons licence, unless indicated otherwise in a credit line to the material. If material is not included in the article's Creative Commons licence and your intended use is not permitted by statutory regulation or exceeds the permitted use, you will need to obtain permission directly from the copyright holder. To view a copy of this licence, visit <http://creativecommons.org/licenses/by/4.0/>.






References

1. Y. Yang, D. Li, C. Li, Y. Liu, K. Jiang, *J. Hazard. Mater.* **341**, 93 (2018)
2. J. Quenneville, R.S. Taylor, A.C.T. van Duin, *J. Phys. Chem. C* **114**(44), 18894 (2010)
3. C.N. Rusu, J.T. Yates, *J. Phys. Chem. B* **104**(51), 12292 (2000)
4. A. Kumar, M. Castro, J.-F. Feller, *Sensors* **23**(8), 4017 (2023)
5. A.D. Wilson, L.B. Forse, *Sensors* **23**(6), 2887 (2023)
6. R.A. Kalel, *Chem. Pap.* **77**(3), 1253 (2023)
7. K. Rumchev, H. Brown, J. Spickett, *Rev. Environ. Health* **22**(1), 39 (2007)
8. H.M. Aliha, A.A. Khodadadi, Y. Mortazavi, *Sens. Actuators B Chem.* **181**, 637 (2013)
9. B. Huang, C. Lei, C. Wei, G. Zeng, *Environ. Int.* **71**, 118 (2014)
10. Y. Wang, Y. Gao, Z. Wang, J. Yan, Y. Chen, *Sens. Actuators B Chem.* **393**, 134219 (2023)
11. M. Khatib, H. Haick, *ACS Nano* **16**(5), 7080 (2022)

12. Z.-H. He, S.-D. Gong, S.-L. Cai, Y.-L. Yan, G. Chen, X.-L. Li, S.-R. Zheng, J. Fan, W.-G. Zhang, *Cryst. Growth Des.* **19**(6), 3543 (2019)
13. C.K. McGinn, Z.A. Lamport, I. Kymissis, *ACS Sens.* **5**(6), 1514 (2020)
14. J. Zheng, H.L. Noh, H.W. Chun, B.M. Oh, J. Lee, S.-K. Choi, E. Kim, D. Jung, W.S. Lee, J.H. Kim, *Sens. Actuators B Chem.* **341**, 130013 (2021)
15. A. Colombelli, M. Serri, M. Mannini, R. Rella, M.G. Manera, *Sens. Actuators B Chem.* **253**, 266 (2017)
16. Z. Kang, D. Zhang, T. Li, X. Liu, X. Song, *Sens. Actuators B Chem.* **345**, 130299 (2021)
17. Y. Zhu, Y. Zhu, J. Xu, *Chin. Chem. Lett.* **34**(1), 107391 (2023)
18. C. Kosslinger, E. Uttenthaler, S. Drost, F. Aberl, H. Wolf, G. Brink, A. Stanglmaier, E. Sackmann, *Sens. Actuators B Chem.* **24**(1–3), 107 (1995)
19. L. Laricchia-Robbio, R.P. Revoltella, *Biosens. Bioelectron.* **19**(12), 1753 (2004)
20. D.A. Parry, M.M. Sallah, L.S. Miller, I.R. Peterson, R. Hollyoak, *Supramol. Sci.* **4**(3–4), 427 (1997)
21. Z. Li, W. Zeng, Q. Li, *Sens. Actuators A* **346**, 113845 (2022)
22. J.N. Wilde, J. Nagel, M.C. Petty, *Thin Solid Films* **327–329**, 726 (1998)
23. T. Çinko, U. Koyuncu, B.C. Ömür, A. Altındal, N. Arsu, *Prog. Org. Coat.* **132**, 125 (2019)
24. S.Q. Memon, N. Memon, A. Mallah, R. Soomro, M.Y. Khuhawar, *Curr. Anal. Chem.* **10**(3), 393 (2014)
25. M. Laajimi, A. Jebnoui, M. Chemli, M. Majdoub, R. Ben Chaabane, *Mater. Chem. Phys.* **228**, 336 (2019)
26. F. Wang, T. Qi, Z. Su, Y. Xie, *J. Mol. Model.* **24**(3), 58 (2018)
27. M.Z. Alam, Alümuddin, S.A. Khan, *J. Fluoresc.* **33**(4), 1241 (2023)
28. M. Kaur, S. Kumar, M. Yusuf, J. Lee, R.J.C. Brown, K.-H. Kim, A.K. Malik, *Coord. Chem. Rev.* **449**, 214214 (2021)
29. T. Han, W. Wei, J. Yuan, Y. Duan, Y. Li, L. Hu, Y. Dong, *Talanta* **150**, 104 (2016)
30. E. Halay, S. Bozkurt, R. Capan, M. Erdogan, R. Unal, Y. Acikbas, *Res. Chem. Intermed.* **46**(10), 4433 (2020)
31. E. Halay, Y. Acikbas, R. Capan, S. Bozkurt, M. Erdogan, R. Unal, *Tetrahedron* **75**(17), 2521 (2019)
32. S. Bozkurt, E. Halay, M. Durmaz, M. Topkafa, Ö. Ceylan, *J. Heterocycl. Chem.* **58**(5), 1079 (2021)
33. E. Halay, *Res. Chem. Intermed.* **47**(10), 4281 (2021)
34. J. Wang, X. Guo, *J. Hazard. Mater.* **390**, 122156 (2020)
35. R. Çapan, I. Çapan, F. Davis, *Sens. Actuators B* **394**, 134463 (2023)
36. Ş Altın, F. Dumludağ, Ç. Oruç, A. Altındal, *Microelectron. Eng.* **134**, 7 (2015)
37. F.C. Wu, R.L. Tseng, R.S. Juang, *Chem. Eng. J.* **150**(2–3), 366 (2009)
38. M. Pişkin, N. Can, Z. Odabaş, A. Altındal, *J. Porphyrins Phthalocyanines* **22**(1–3), 189 (2018)
39. E. Ay, *CBU J. Sci.* **12**(3), 375 (2016)
40. K.A. Abdalkarim, S.J. Mohammed, A.H. Hasan, K.M. Omer, F. Paularokiadoss, R.F. Hamarouf, K. Hikmat, H. Aziz, H.Q. Hassan, T.C. Jeyakumar, *Chem. Phys. Impact* **8**, 100402 (2024)
41. D.I. Tofiq, H.Q. Hassan, K.A. Abdalkarim, *Arabian J. Chem.* **14**(12), 103429 (2021)
42. A.N. Kursunlu, Y. Acikbas, C. Yilmaz, M. Ozmen, I. Capan, R. Capan, K. Buyukkabasakal, A. Senocak, *A.C.S. Appl. Mater. Interfaces* **16**, 31851 (2024)
43. L. Largette, R. Pasquier, *Chem. Eng. Res. Des.* **109**, 495 (2016)
44. E.D. Pusfitasari, J. Ruiz-Jimenez, J. Samuelsson, V. Besel, T. Fornstedt, K. Hartonen, M.-L. Riekola, *J. Chromatogr. A* **1703**, 464119 (2023)
45. A.-L. Cheng, W.-L. Huang, *Org. Geochem.* **35**(4), 413 (2004)

Publisher's Note Springer Nature remains neutral with regard to jurisdictional claims in published maps and institutional affiliations.

Authors and Affiliations

Erkan Halay^{1,2}  · Inci Capan³  · Rifat Capan³  · Emriye Ay⁴  ·
Yaser Acikbas⁵ 

✉ Yaser Acikbas
yaser.acikbas@usak.edu.tr

Erkan Halay
erkan.halay@usak.edu.tr

Inci Capan
inci.capan@gmail.com

Rifat Capan
rcapan@balikesir.edu.tr

Emriye Ay
emriye.ay@cbu.edu.tr

¹ Department of Chemistry, Scientific Analysis Technological Application and Research Center, Usak University, 64200 Usak, Turkey

² Department of Chemistry and Chemical Processing Technologies, Banaz Vocational School, Usak University, 64500 Usak, Turkey

³ Department of Physics, Faculty of Arts and Science, University of Balikesir, 10145 Balikesir, Turkey

⁴ Department of Tobacco Technology Engineering, School of Tobacco Expertise, University of Manisa Celal Bayar, Manisa 45200, Turkey

⁵ Department of Materials Science and Nanotechnology Engineering, Usak University, 1 Eylul Campus, 64200 Usak, Turkey